Inverse Problems and Imaging
Volume 7, No. 2, 2013, x–xx
doi:10.3934/ipi.2013.7.xx

A THREE-DIMENSIONAL INVERSE GRAVIMETRY PROBLEM FOR ICE WITH SNOW CAPS

Victor Isakov

Department of Mathematics and Statistics
Wichita State University
Wichita, Kansas 67260, USA

Shingyu Leung and Jianliang Qian

Department of Mathematics
Hong Kong University of Science and Technology
Clear Water Bay, Hong Kong, China
and
Department of Mathematics
Michigan State University
East Lansing, MI 48824, USA

(Communicated by Mikko Salo)

Abstract. We propose a model for the gravitational field of a floating iceberg D with snow on its top. The inverse problem of interest in geophysics is to find D and snow thickness g on its known (visible) top from remote measurements of derivatives of the gravitational potential. By modifying the Novikov's orthogonality method we prove uniqueness of recovering D and g for the inverse problem. We design and test two algorithms for finding D and g. One is based on a standard regularized minimization of a misfit functional. The second one applies the level set method to our problem. Numerical examples validate the theory and demonstrate effectiveness of the proposed algorithms.

1. **Formulation.** The Newtonian potential of a (Radon) measure μ is

$$u(x;\mu)=\int_{\Omega}\Phi(x,y)d\mu(y), \tag{1}$$

where

$$\Phi(x,y)=\frac{1}{4\pi|x-y|}.$$

We will assume that μ is zero outside $\bar{D}\subset\Omega$, D is some bounded open set, Ω is a given open set in $\mathbb{R}^3$, and $\Gamma_0\subset\partial\Omega$.

The inverse problem of gravimetry

Find μ given

$$G_\alpha=\partial^\alpha u(\cdot;\mu),\alpha\in\mathcal{A}\text{ on }\Gamma_0, \tag{2}$$

where $\mathcal{A}$ is a set of multiindices α. Here $u(\cdot;\mu)$ is the function defined as $u(x;\mu)$ at a point x.

A first crucial question is whether there is enough data to (uniquely) find μ. Unfortunately, there is a very large (infinite dimensional) manifold of solutions to

2010 *Mathematics Subject Classification.* 65N21, 65N06, 65N80.
Key words and phrases. Inverse gravimetry, level set method, alternating minimization, weighted essentially non-oscillatory schemes, Green function.

the inverse problem of gravimetry. Indeed, let u_0 be a function in the Sobolev space $H^2(\Omega)$ which is zero in $\mathbb{R}^3 \setminus D$, and let $f_0 = -\Delta u_0$. Then $u(\cdot; f_0 dm) = u_0$ (dm is the Lebesgue measure) in $\mathbb{R}^3$, and hence $u(\cdot; f_0 dm)$ has zero data (2). Obviously, $u(\cdot;\mu)$ and $u(\cdot;\mu) + u(\cdot; f_0 dm)$ have the same data (2) on Γ_0, so μ and $\mu + f_0 dm$ produce the same data (2), but they are different in Ω.

Another feature of the inverse problem of gravimetry is its severe ill conditioning. The (compact) linear operator mapping μ into the data (2) has exponentially fast decreasing singular values. This decay is growing with the distance from Γ_0 to D. When Ω is a sphere of radius R and D is a concentric sphere of radius r these singular values behave like the exponential powers of $\frac{r}{R}$. A rigorous analysis of this operator in $\mathbb{R}^2$ in some practically important cases (Ω is a lower half plane and Γ is an interval) was given in a recent paper [7], where it is demonstrated that one can only expect to find four to seven parameters describing μ.

In this paper we consider $\mu = \chi_D dm + g d\Gamma$ which models a (sea) ice domain D with snow covering a part Γ of the upper boundary of D and inducing a density distribution g on Γ. In section 2 we briefly review available uniqueness results for the inverse gravimetry problem and demonstrate uniqueness of recovering the x_3-convex D and g on Γ (a known "visible" part of ∂D). Proofs use the Novikov's orthogonality method [17] and some new ingredients. In section 3 we design and implement two new numerical algorithms for finding (D, g) from (2) and test these algorithms on geophysically meaningful examples. One of the algorithms is based on the level set method which was used recently for a different inverse gravimetry problem in [11].

2. Uniqueness results.

To regain uniqueness one has to restrict unknown distributions to a smaller, physically meaningful uniqueness class.

Let Ω be bounded. One can look for f with the smallest $L^2(\Omega)$-norm. The subspace of harmonic functions f_h in Ω is $L^2(\Omega)$-closed, so for any $f \in L^2(\Omega)$ there is a unique f_h such that $f = f_h + f_0$, where f_0 is L^2-orthogonal to f_h. Since $\Phi(x, y)$ is a harmonic function of $y \in \Omega$ when x is outside Ω, $u(\cdot; f_0 dm) = 0$ outside Ω. Hence the harmonic orthogonal component f_h of f has the same exterior data and the minimal L^2-norm. It is not hard to show that for Lipschitz Ω this f_h is unique [10]. The equation $-\Delta u(\cdot; f_h dm) = f_h$ implies the biharmonic equation $\Delta^2 u(\cdot; f_h dm) = 0$ in Ω. When $\Gamma_0 = \partial\Omega$ and we are given u and the normal derivatives $\partial_\nu u$ on Γ_0, we have a well-posed first boundary-value problem for the biharmonic equation for $u(\cdot; f_h dm)$. Solving this problem we find f_h. However, it is hard to interpret f_h (geo)physically and knowing f_h does not help much with finding f either.

A (geo)physical intuition suggests looking for a perturbing inclusion D of constant density, i.e. for $\mu = \chi_D dm$ (a characteristic function of the set D).

Since (in distributional sense) $-\Delta u(\cdot;\mu) = \mu$ in Ω, by using the Green's formula (or the definition of a weak solution) we have

$$-\int_\Omega v d\mu = \int_{\partial\Omega} ((\partial_\nu u)v - (\partial_\nu v)u) \tag{3}$$

for any function $v \in H^1(\Omega)$ which is harmonic in a bounded Lipschitz domain Ω, where ν is the outward normal to the boundary of Ω. If $\Gamma_0 = \partial\Omega$, then the right handed side in (3) is known so that we are given all harmonic moments of μ. In particular, letting $v = 1$ we obtain the total mass of μ, and by taking v to be

coordinate (linear) functions we obtain moments of μ of first order, and hence the center of gravity of μ.

Even when one assumes that $\mu = \chi_D dm$, there is non uniqueness due to possible disconnectedness of the complement of D. To explain it, we recall that if D is the ball $B(a,R)$ with center a of radius R then its Newtonian potential $u(x;\chi_D dm) = M\frac{1}{4\pi|x-a|}$, where M is the total mass of D. So for any constant C and $R_1^3 - R_2^3 = C$ the exterior potentials of all annuli $B(a,R_1) \setminus B(a,R_2)$ are the same. By using this simple example and some reflections in $\mathbb{R}^n$ one can find two different domains with connected boundaries and equal exterior Newtonian potentials. An additional condensation of singularities argument from the theory of functions of complex variables creates a continuum of different domains with connected boundaries and the same exterior potential [10]. So there is a need in imposing some geometrical conditions on D.

A domain D is called star shaped with respect to a point a if any ray originated at a intersects D over an interval. An open set D is x_j-convex if any straight line parallel to the x_j-axis intersects D over an interval.

In Theorems 2.1-2.4 we assume that Γ_0 is a (nonempty) Lipschitz surface in $\mathbb{R}^3$.

Theorem 2.1. *Let D_1 and D_2 be two star-shaped Lipschitz domains with respect to their centers of gravity or two x_j-convex Lipschitz domains in $\mathbb{R}^3$. Let u_1 and u_2 be potentials of D_1 and D_2, respectively.*

If the normal derivatives are equal, $\partial_\nu u_1 = \partial_\nu u_2$ on Γ_0, then $D_1 = D_2$, where ν is the outward normal to the boundary Γ_0.

This result is proven in [10] by the Novikov's orthogonality method which we will demonstrate to prove our new Theorem 2.4 below.

In Theorems 2.2-2.4 we assume that $\{\alpha : |\alpha| = 1\} \subset \mathcal{A}$, i.e. that we are given at least ∇u on Γ_0.

In some applications a part of boundary, $\Gamma \subset \partial D$, is known while the density f needs to be determined.

Theorem 2.2. *Let $D = \{x : (x_1,x_2) \in \Gamma', d(x_1,x_2) < x_3 < \gamma(x_1,x_2)\}$ be a Lipschitz domain and its density $f \in C(\mathbb{R}^3)$ does not depend on x_3; $D \subset suppf$; let the upper surface of D, $\Gamma = \{(x_1,x_2,\gamma(x_1,x_2)) : (x_1,x_2) \in \Gamma'\}$ be known, where Γ' is a known open domain in $\mathbb{R}^2$, $\gamma \in Lip$ is a known function, and $d \in Lip$ is an unknown function.*

Then the data (2) for $\mu = f\chi_D dm$ uniquely determine D and f on Ω.

A proof is in [10], Theorem 3.2.1.

Theorem 2.3. *Let $D = \{x : (x_1,x_2) \in \Gamma', d(x_1,x_2) < x_3 < \gamma(x_1,x_2)\}$ be a Lipschitz domain in $\mathbb{R}^3$ and its density $f \in C(\mathbb{R}^3)$ depends only on x_3; $D \subset suppf$, where Γ' is a known open domain in $\mathbb{R}^2$, $\gamma \in Lip$ is a known function, and $d \in Lip$ is an unknown function.*

Then the data (2) for $\mu = f\chi_D dm$ uniquely determine D and f on Ω.

This is a particular case of Theorem 3.2.2 in [10].

For further results on inverse problems of gravimetry, we refer to Isakov [10] and Prilepko[19].

Now we give a new uniqueness result.

Let $D = \{x : d(x_1,x_2) < x_3 < d^+(x_1,x_2)\}$ be a Lipschitz open bounded set. Let $x' = (x_1,x_2)$ be the projection of $x = (x_1,x_2,x_3)$ onto the (x_1,x_2) plane and S'

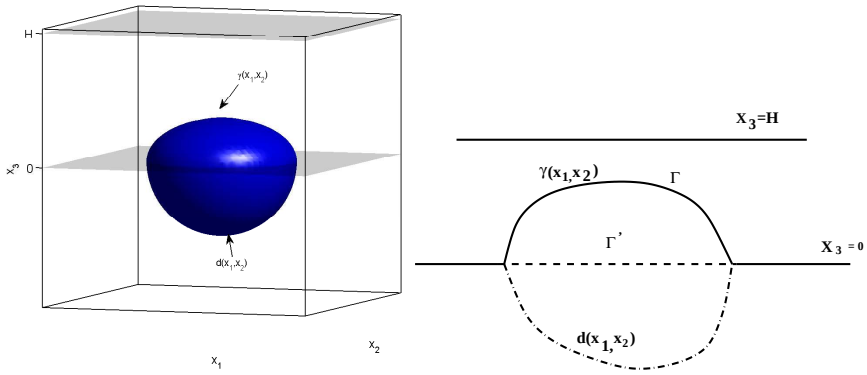

FIGURE 1. Illustration of ice with snow cap.

be the projection of the set $S \subset \mathbb{R}^3$. We will assume that any point $x \in \partial D$ with $x' \in P_0$, where P_0 is a subset of zero (Lebesgue) measure in $\mathbb{R}^2$, satisfies the cone condition. The cone condition [10] means that there are an open cone with vertex at x and a neighborhood V of x such that $\partial D \cap V$ does not intersect this cone. Any D with piecewise C^1 boundary satisfies this condition.

The unknown d and d^+ describe the shape of the floor/ice,

$$\Gamma = \{(x_1, x_2, \gamma(x_1, x_2)), (x_1, x_2) \in \Gamma'\}$$

is a known upper part of ∂D, and $\Gamma_0 = \{x : x_3 = H\}$ (airborne/satellite measurements). Here $\gamma = d^+$ on Γ'. In applications, the upper part Γ of the unknown domain D is covered by a relatively thin layer of snow. The single layer $gd\Gamma$ of density $g \in L^1(\Gamma)$ on Γ is an approximation of this thin volume of snow.

Theorem 2.4. *Let both $\gamma \in C^{1+\lambda}$ with $(0 < \lambda < 1)$ and Γ' be known. Then the data (2) for $\mu = gd\Gamma + \chi_D dm$ uniquely determine g (thickness of snow) on Γ and D.*

In the proof we will use solvability and stability (with respect to a domain) of a mixed oblique derivative problem for harmonic functions. We will collect some needed preliminary results. Let Ω_1 be a bounded domain with the boundary which consists of two disjoint closed $C^{1+\lambda}$ surfaces Γ_1 and Γ_2. Let l be a $C^{1+\lambda}$ (nonzero) vector field on Γ_1 which is not tangential to Γ_1. Referring to the classical method of integral equations and maximum principles [16] we claim that for any $C^{1+\lambda}(\Gamma_2)$-function u_0, there is a unique solution $u \in C^{1+\lambda}(\bar{\Omega}_1)$ to the mixed elliptic boundary value problem

$$\Delta u = 0 \text{ in } \Omega_1, \ \nabla u \cdot l = 0 \text{ on } \Gamma_1, \ u = u_0 \text{ on } \Gamma_2. \tag{4}$$

Moreover, maximum and minimum of this solution are achieved on Γ_2.

Now we briefly describe approximation and stability results (with respect to a domain) which are given in the original paper [12] and summarized in [10], section 1.7, in the case of the Dirichlet problem, i.e. when Γ_1 is void. Let Ω_{1n} be the sequence of domains described above, $\Omega_{1,n+1} \subset \Omega_{1,n}$, where the boundaries $\Gamma_{1,n}$ with the oblique derivative data are the same for all $\Omega_{1,n}$ while the boundaries $\Gamma_{2,n}$ vary. Let Ω_{1*} be the intersection of $\{\Omega_{1,n}\}$ and its boundary consist of the disjoint parts $\Gamma_{1*} \subset \Gamma_{1,n}$ and $\Gamma_{2*} \subset \Omega_{1,n}$. Let $u_0 \in C^{1+\lambda}(\mathbb{R}^3)$ and let u_n be the solution

to the boundary value problem (4) in $\Omega_{1,n}$. If a point $x \in \Gamma_{2*}$ satisfies the exterior cone condition with respect to Ω_{1*}, then there is $\lim_n u_n(x) = u_0(x)$. Proofs follow the arguments in [12] which are based only on maximum principles, solvability of the Dirichlet problem in smooth domains, and local arguments using barriers. All these tools are available in our case.

Proof. Let (D_1, g_1) and (D_2, g_2) generate the same data (2), but $D_1 \neq D_2$. Let D_* be the smallest (open) x_3-convex set containing $D_1 \cup D_2$. The function $u(; \chi_{D_2} dm + g_2 d\Gamma - \chi_{D_1} dm - g_1 d\Gamma)$ has zero Cauchy data on Γ_0 and is harmonic outside $\bar{D}_*$. Hence this function is zero outside $\bar{D}_*$. From (3) with $\mu = \chi_{D_2} dm + g_2 d\Gamma - \chi_{D_1} dm - g_1 d\Gamma$ we obtain

$$\int_{D_1} v + \int_\Gamma v g_1 d\Gamma = \int_{D_2} v + \int_\Gamma v g_2 d\Gamma \tag{5}$$

for any function v which is harmonic near $\bar{D}_*$. Letting h be harmonic near $\bar{D}_*$, it follows that $v = \partial_3 h$ is also harmonic there and hence

$$\int_{D_1} \partial_3 h + \int_\Gamma \partial_3 h g_1 d\Gamma = \int_{D_2} \partial_3 h + \int_\Gamma \partial_3 h g_2 d\Gamma \tag{6}$$

for all h harmonic near $\bar{D}_*$.

Let D_{1*} be a domain containing D_* with $\bar{D}_* \subset D_{1*} \cup \Gamma$, $\partial D_{1*} \in C^{1+\lambda}$, and $\Gamma \subset \partial D_{1*}$. To get a contradiction we would like to use h satisfying the following conditions

$$\Delta h = 0 \text{ in } D_{1*},\ \partial_3 h = 0 \text{ on } \Gamma,\ \ h \in C^1(\bar{D}_{1*}). \tag{7}$$

Since Γ is the graph of a C^1-function $x_3 = \gamma(x')$, for small $\delta > 0$ the translation $h(x', x_3 - \delta)$ is harmonic near $\bar{D}_*$; so we have for this translation the orthogonality relation (6). Letting in this relation $\delta \to 0$ we conclude that

$$\int_{D_1} \partial_3 h = \int_{D_2} \partial_3 h \tag{8}$$

for all h satisfying (7).

In the proof we can assume that $D_1 \not\subseteq D_2$ and $D_2 \not\subseteq D_1$. Indeed, let $D_1 \subset D_2$. Let v solve the Dirichlet problem $\Delta v = 0$ in D_{1*} with $v = u_0$ on ∂D_{1*}, where $u_0 \in C(\mathbb{R}^3)$, $u_0 = 0$ on Γ, and $0 < u_0$ on $\partial D_{1*} \setminus \Gamma$. By maximum principles $0 < v$ in D_{1*}. Using this v in the orthogonality relation (5) we obtain a contradiction: the left handed side will be less than the right handed side.

We will subdivide $P = D'_*$ into the following sets,

$$P_1 = \{d_1 \le d_2, d_1^+ \le d_2^+\} \setminus \Gamma',\ P_2 = \{d_2 < d_1, d_1^+ \le d_2^+\} \setminus \Gamma',$$
$$P_3 = \{d_2 \le d_1, d_2^+ < d_1^+\},\ P_4 = \{d_1 < d_2, d_2^+ < d_1^+\},$$
$$P_5 = \{d_1 \le d_2\} \cap \Gamma',\ P_6 = \{d_2 < d_1\} \cap \Gamma'.$$

Up to a relabelling of D_1 and D_2, we may assume that there is a ball B centered at a point of ∂D_2 such that $\bar{B} \subset D_*$. Using relabelling if needed we have the following **three Cases**: 1) $B' \subset P_1$, 2) $B' \subset P_3$, or 3) $B' \subset P_5$.

In the remainder of the proof we will replace the Laplace equation by another elliptic equation with a strict maximum principle. Let $0 < w$, $\Delta v < 0$ near $\bar{D}_*$, and $w \in C^2$ which does not depend on x_3. We can choose $w(x) = 1 - \delta(x_1^2 + x_2^2)$ with δ a small positive constant. We will use the substitution $h = wu$. Then the Laplace equation (7) is equivalent to the elliptic equation $Au = 0$ whose solutions satisfy the strict maximum principle. Here $Au = w\Delta u + 2\nabla w \cdot \nabla u + \Delta w u$.

Integrating by parts in (8) and introducing the notation $u(x';d) = u(x', d(x'))$, we obtain

$$\int_P w(u(;d_2^+) - u(;d_2) - u(;d_1^+) + u(;d_1)) = 0 \tag{9}$$

for all u satisfying

$$Au = 0 \text{ in } D_{1*},\ \partial_3 u = 0 \text{ on } \Gamma, u \in C^1(\bar{D}_{1*}). \tag{10}$$

Using the remarks concerning solutions to (4), we conclude that for any function $u_0 \in C^{1+\lambda}(\mathbb{R}^3)$, $0 \le u_0 \le 1$, there is a function u, $0 \le u \le 1$, which is a pointwise limit of functions u_k, $k = 1, 2, \cdots$, satisfying (10). Moreover, $\lim u_k(x^0) = u_0(x^0)$ as $k \to +\infty$ at any point $x^0 \in \partial D_* \setminus \Gamma$ with $x^{0'} \in D'_* \setminus P_0$, where P_0 is a set of zero Lebesgue measure in $\mathbb{R}^2$. Since C^2-functions are dense in L^1, one can find a sequence of functions $u_{0k} \in C^2(\mathbb{R}^3), 0 \le u_{0k} \le 1$, such that

$$u_{0k}(;d_2^+) \to 1 \text{ in } L^1(P_1 \cup P_2), u_{0k}(;d_1^+) \to 0 \text{ in } L^1(P_3 \cup P_4),$$
$$u_{0k}(;d_1) \to 1 \text{ in } L^1(P_1 \cup P_4 \cup P_5), u_{0k}(;d_2) \to 0 \text{ in } L^1(P_2 \cup P_3 \cup P_6).$$

Hence there are functions $u_k \in C^{1+\lambda}(D_* \cup \Gamma)$ satisfying (10) such that

$$u_k(;d_2^+) \to 1 \text{ in } L^1(P_1 \cup P_2), u_k(;d_1^+) \to 0 \text{ in } L^1(P_3 \cup P_4),$$
$$u_k(;d_1) \to 1 \text{ in } L^1(P_1 \cup P_4 \cup P_5), u_k(;d_2) \to 0 \text{ in } L^1(P_2 \cup P_3 \cup P_6). \tag{11}$$

Moreover,

$$0 \le u_k \le 1 \text{ on } \bar{D}_*,\ u_k < 1 - \varepsilon_0 \text{ on } B \tag{12}$$

for some $\varepsilon_0 > 0$ which does not depend on k. Indeed the inequalities in D_* follow from maximum principles. To obtain the inequality on B, let B^* be a ball with $\bar{B}^* \subset D_*$ and $\bar{B} \subset B^*$. Let u^* solve the following Dirichlet problem: $Au^* = 0$ in B^*, and $u^* = 1$ on ∂B^*. By the strict maximum principle $u^* < 1 - \varepsilon_0$ on B for some (small) positive ε_0. By maximum principles $u_k \le 1$ on D_* and hence $u_k \le u^* < 1 - \varepsilon_0$ on B.

We first consider **Case 1)**. Due to (11) and (12) the lower limit of the integrals (9) over P_1 is equal to

$$\liminf \int_{P_1} w(1 - u_k(;d_2) - u_k(;d_1^+) + 1)$$
$$\ge \int_{P_1 \setminus B'} (1 - 1 - 1 + 1) + \int_{B'} (1 - (1 - \varepsilon_0) - 1 + 1) > 0\,.$$

The lower limit of the integrals (9) over P_2 is equal to

$$\liminf \int_{P_2} w(1 - 0 - u_k(;d_1^+) + u_k(;d_1)) \ge 0\,,$$

due to (12). The lower limit of the integrals (9) over P_3 is equal to

$$\liminf \int_{P_2} w(u_k(;d_2^+) - 0 - 0 + u_k(;d_1)) \ge 0\,,$$

again due to (12). The lower limit of the integrals (9) over P_5 is equal to

$$\liminf \int_{P_2} w(-u_k(;d_1^+) + 1) \ge 0\,,$$

again due to (12).

Similarly, the lower limits of the integrals (9) over P_3, P_4, and P_6 are non negative.

In **Case 2)**, due to (11) and (12), the lower limit of the integrals (9) over P_3 is equal to

$$\begin{aligned} &\liminf \int_{P_3} w(u_k(;d_2^+) - u_k(;d_2) - 0 + 1) \\ \geq \quad &\int_{P_3 \setminus B'} (0 - 1 - 0 + 1) + \int_{B'} (\varepsilon_0 - 1 - 0 + 1) > 0\,. \end{aligned}$$

As above the limits of the integrals over P_1, P_2, P_4, P_5, and P_6 are non negative.

In **Case 3)**, due to (11) and (12), the lower limit of the integrals (9) over P_5 is equal to

$$\begin{aligned} &\liminf \int_{P_5} w(-u_k(;d_2) + 1) \\ \geq \quad &\int_{P_5 \setminus B'} (-1 + 1) + \int_{B'} ((-1 + \varepsilon_0) + 1) > 0\,. \end{aligned}$$

As above the limits of the integrals over P_1, P_2, P_4, and P_6 are non negative.

So the lower limit of the integrals (9) with $u = u_k$ as $k \to +\infty$ is positive and we have a contradiction with (9).

When $D_1 = D_2$, by using completeness of v in $L_\infty(\Gamma)$ (section 1.8 in [10]) we conclude from (5) that $g_1 = g_2$.

The proof is complete. □

Remark. If $\mu = \chi_D dm + g d\Gamma$, $y = (y_1, y_2, y_3)$, then the potential

$$\begin{aligned} u(x;\mu) \quad &= \quad \int_\Omega \Phi(x,y)\chi_D(y)dy + \int_\Gamma \Phi(x,y)g(y)d\Gamma(y) \qquad (13) \\ &= \quad \int_{D'} \left(\int_{d(y_1,y_2)}^{d^+(y_1,y_2)} \Phi(x,y)dy_3 \right) dy_1 dy_2 \\ &+ \quad \int_{\Gamma'} \Phi(x,(y_1,y_2,\gamma(y_1,y_2)))g(y_1,y_2,\gamma(y_1,y_2))J(y_1,y_2)dy_1dy_2 \qquad (14) \end{aligned}$$

where $J(y_1, y_2) = \sqrt{1 + |\nabla\gamma(y_1, y_2)|^2}$ is the Jacobian.

3. Numerical methods.

We propose two strategies to carry out the above inversion process: one is a direct approach, and the other is a level set approach. In the first approach, we assume that the unknown surface $d(y_1, y_2)$ has known topology and there will be no merging or splitting of the surface. This method can deal with simple objects. A more realistic example, unfortunately, might involve unknown topology under water. For example, from multiple objects observed above the sea surface, the numerical approach should be able to detect if there is any connectivity of these icebergs under the sea surface. In the second part of this section, we propose a level set approach which can easily handle such a situation.

3.1. A direct approach.

Since $\mu = \chi_D dm + g d\Gamma$, we need to determine functions d, d^+ and g. We will assume that the functions d and d^+ are defined on an open subset Γ_* of $\mathbb{R}^2$ containing D' and that the function g does not depend on x_3. We let $d = d^+$ on $\Gamma_* \setminus D'$. We consider the following measurement data:

$$\nabla u(x; \chi_D dm + g d\Gamma) = \mathbf{g}(x),\ x \in \Gamma_0.$$

To find d, d^+ and g we solve the following minimization problem:

$$\min_{d,d^+,g} F(d,d^+,g) = \min_{d,d^+,g} \|\nabla u(\cdot;\chi_D dm + g d\Gamma) - \mathbf{g}\|^2_{L^2(\Gamma_0)}\,. \tag{15}$$

To that end we calculate the Frechet derivatives of the functional $F(d,d^+,g)$ with respect to d, d^+ and g:

$$\begin{aligned} & F(d+d_1, d^+ + d_1^+, g+g_1) - F(d,d^+,g) \\ = \quad & \left(\frac{\partial F}{\partial d}, d_1\right)(\Gamma_*) + \left(\frac{\partial F}{\partial d^+}, d_1^+\right)(\Gamma_*) + \left(\frac{\partial F}{\partial g}, g_1\right)(\Gamma') + O(d_1^2 + d_1^{+2})\,. \end{aligned}$$

Here $(f,d)(\Gamma_*)$ is the standard scalar product in $L^2(\Gamma_*)$. To simplify notations, we introduce

$$G(x;d,d^+,g) = \nabla u(x;\chi_D dm + g d\Gamma) - \mathbf{g}(\mathbf{x})\,. \tag{16}$$

Thus

$$\begin{aligned} & G(x;d+d_1,d^+ + d_1^+, g+g_1) \\ = \quad & G(x;d,d^+,g) + \int_{\Gamma_*}\int_{d(y_1,y_2)+d_1(y_1,y_2)}^{d(y_1,y_2)} \nabla_x \Phi(x,y) dy_3 dy_1 dy_2 \\ & + \int_{\Gamma_*}\int_{d^+(y_1,y_2)}^{d(y_1,y_2)+d_1^+(y_1,y_2)} \nabla_x \Phi(x,y) dy_3 dy_1 dy_2 \\ & + \int_{\Gamma'} \nabla_x \Phi(x,(y_1,y_2,\gamma(y_1,y_2))) g_1(y_1,y_2) J(y_1,y_2) dy_1 dy_2 \\ = \quad & G(x;d,d^+,g) - \int_{\Gamma_*} \nabla_x \Phi(x,y_1,y_2,d(y_1,y_2)) d_1(y_1,y_2) dy_1 dy_2 \\ & + \int_{\Gamma_*} \nabla_x \Phi(x,y_1,y_2,d^+(y_1,y_2)) d_1^+(y_1,y_2) dy_1 dy_2 \\ & + \int_{\Gamma'} \nabla_x \Phi(x,y_1,y_2,\gamma(y_1,y_2)) g_1(y_1,y_2) J(y_1,y_2) dy_1 dy_2 + \cdots \\ = \quad & G(x;d,g) + G_1(x;d,d_1) + G_2(x;d^+,d_1^+) + G_3(x;g_1) + \cdots\,, \end{aligned} \tag{17}$$

where $\cdots$ denotes terms bounded by $C(|d_1|^2 + |d_1^+|^2)$, and

$$\begin{aligned} G_1(x;d,d_1) &= -\int_{\Gamma_*} \nabla_x \Phi(x,y_1,y_2,d(y_1,y_2)) d_1(y_1,y_2) dy_1 dy_2 \\ G_2(x;g,g_1) &= \int_{\Gamma_*} \nabla_x \Phi(x,(y_1,y_2,d^+(y_1,y_2))) d_1^+(y_1,y_2) dy_1 dy_2, \\ G_3(x;g_1) &= \int_{\Gamma'} \nabla_x \Phi(x,y_1,y_2,\gamma(y_1,y_2)) g_1(y_1,y_2) J(y_1,y_2) dy_1 dy_2. \end{aligned}$$

So

$$\begin{aligned}
& F(d+d_1, d^+ + d_1^+, g+g_1) - F(d, d^+, g) \\
= & \int_{\Gamma_0} G^T(x; d+d_1, d^+ + d_1^+, g+g_1) G(x; d+d_1, d^+ + d_1^+, g+g_1) d\Gamma_0(x) \\
& - \int_{\Gamma_0} G^T(x; d, d^+, g) G(x; d, d^+, g) d\Gamma_0(x) \\
= & \ 2 \int_{\Gamma_0} G^T(x; d, d^+, g)(G_1(x; d, d_1) + G_2(x; d^+, d_1^+) + G_3(x; g_1)) d\Gamma_0(x) + ... \\
= & \int_{\Gamma_*} \left(2 \int_{\Gamma_0} G^T(x; d, d^+, g) \nabla_x \Phi(x, y, d(y)) d\Gamma_0(x) \right) d_1(y) dy_1 dy_2 \\
& + \int_{\Gamma_*} \left(2 \int_{\Gamma_0} G^T(x; d, d^+, g) \nabla_x \Phi(x, y_1, y_2, d^+(y)) d\Gamma_0(x) \right) d_1^+(y) dy_1 dy_2 \\
& + \int_{\Gamma'} \left(2 \int_{\Gamma_0} G^T(x; d, d^+, g) \nabla_x \Phi(x, y, \gamma(y)) J(y) d\Gamma_0(x) \right) g_1(y) dy_1 dy_2 \\
& + \cdots,
\end{aligned}$$

where $y = (y_1, y_2)$. Therefore, the Frechet derivatives are given by

$$\begin{aligned}
\frac{\partial F}{\partial d} &= 2 \int_{\Gamma_0} G^T(x; d, d^+, g) \nabla_x \Phi(x, (y_1, y_2, d(y_1, y_2))) d\Gamma_0(x), \\
\frac{\partial F}{\partial d^+} &= 2 \int_{\Gamma_0} G^T(x; d, d^+, g) \nabla_x \Phi(x, (y_1, y_2, d^+(y_1, y_2))) d\Gamma_0(x), \\
\frac{\partial F}{\partial g} &= 2 \int_{\Gamma_0} G^T(x; d, d^+, g) \nabla_x \Phi(x, (y_1, y_2, \gamma(y_1, y_2))) J(y_1, y_2) d\Gamma_0(x).
\end{aligned}$$

The necessary conditions for the triple (d, d^+, g) to be a minimizer are that

$$\frac{\partial F}{\partial d} = 0\,, \ \frac{\partial F}{\partial d^+} = 0 \ \text{ and } \ \frac{\partial F}{\partial g} = 0\,.$$

To obtain these minimizers, we use the method of gradient descent by considering the gradient flows

$$\frac{\partial d}{\partial t} = -\frac{\partial F}{\partial d}\,, \ \frac{\partial d^+}{\partial t} = -\frac{\partial F}{\partial d^+} \ \text{ and } \ \frac{\partial g}{\partial t} = -\frac{\partial F}{\partial g},$$

and we solve the above equations to steady states by letting t go to infinity.

In practice, the shape of the iceberg should have certain regularity. We impose the following regularization in the energy so that the lower part of the iceberg is smooth for some $\alpha > 0$

$$\min_{d, d^+, g} F_\alpha(d, d^+, g) = \min_{d, d^+, g} \|\nabla u(\cdot; d, d^+, g) - \mathbf{g}\|^2_{L^2(\Gamma_0)} + \alpha(\|\nabla d\|^2_{L^2} + \|\nabla d^+\|^2_{L^2})\,. \tag{18}$$

3.2. **A level set approach.** As discussed earlier, the above approach assumes that the topology of the lower iceberg surface is known and can be expressed as a function of x_1 and x_2. To relax these assumptions, we follow our previous work proposed in [11] using the level set method. For inverse (obstacle) problems the level set method has been first used by Santosa [23]. Later on, there are many efforts to analyze this method and extend this beautiful idea to a variety of inverse problems; see [26, 14, 3, 9, 4, 6] and references therein. More recently, a level set method was applied to identification of a characteristic function of a domain in the

source term of the Poisson equation from the Cauchy data on the whole boundary of the reference domain Ω [24].

To parameterize the unknown domain D, we will introduce a level set function φ which is Lipschitz continuous and

$$\begin{aligned} \varphi &> 0 \quad \text{on } D, \\ \varphi &= 0 \quad \text{on } \partial D, \\ \varphi &< 0 \quad \text{on } x \in \bar{D}^c. \end{aligned}$$

Since the upper surface of the iceberg is given, the level set function φ must satisfy the condition

$$\varphi(x_1, x_2, \gamma(x_1, x_2)) = 0, \text{ when } x' \in \Gamma' .$$

According to the gravity force relation we define the following operator:

$$A(\varphi, g)(x) = \nabla_x u(x; \chi_D dm + g d\Gamma), \ x \in \Gamma_0. \tag{19}$$

Observe that

$$\begin{aligned} \nabla_x u(x; \chi_D dm + g d\Gamma) &= \int_D \nabla_x \Phi(x, y) dy + \int_\Gamma g(y) \nabla_x \Phi(x, y) d\Gamma(y) \\ &= \int_\Omega \nabla_x \Phi(x, y) H(\varphi(y)) dy + \int_\Gamma g(y) \nabla_x \Phi d\Gamma(y) , \end{aligned} \tag{20}$$

where H is the Heaviside function.

In [11], we have proposed a level set formulation for the inverse problem of finding D when Γ is void. Now we extend this approach to find both D and g. We have to find D and g so that the given gravity data $\mathbf{g}$ satisfies

$$\nabla u(\cdot; \chi_D dm + g d\Gamma) = \mathbf{g} \text{ on } \Gamma_0 .$$

Consequently, the inverse problem is stated as finding D represented by φ such that $A(\varphi, g) = \mathbf{g}$. Furthermore, we will be looking for minimum points (φ, g) of the minimization problem:

$$\min F(\phi, g) = \min \|A(\phi, g) - \mathbf{g}\|^2_{L^2(\Gamma_0)} . \tag{21}$$

To that end we compute the Frechet derivative of the functional $F(\phi, g)$ with respect to ϕ by fixing g:

$$F(\phi + \phi_1, g) - F(\phi, g) = \left(\frac{\partial F}{\partial \phi}, \phi_1 \right) (\Omega) + O(\phi_1^2) .$$

To simplify the calculation, we introduce the mismatch function

$$G(x; \phi, g) = \int_\Omega \nabla_x \Phi(x, y) \ H(\phi(y)) dy + \int_\Gamma g(y) \nabla_x \Phi(x, y) d\Gamma(y) - \mathbf{g}(x) . \tag{22}$$

Then

$$G(x; \phi + \phi_1, g) = G(x; \phi, g) + \int_\Omega \nabla_x \Phi(x, y) \ H'(\phi(y)) \phi_1(y) dy + ...$$

and we have

$$\begin{aligned} & F(\phi+\phi_1,g)-F(\phi,g) \\ = & \int_{\Gamma_0} G^T(x;(\phi+\phi_1,g)G(x;(\phi+\phi_1),g)-G^T(x;(\phi,g))G(x;(\phi,g)))dx \\ = & \int_{\Gamma_0} 2G^T(x;\phi,g)\left(\int_\Omega \nabla_x\Phi(x,y)\ H'(\phi(y))h(y)dy\right)dx+... \\ = & \int_\Omega\left(\int_{\Gamma_0} 2G^T(x;\phi,g)\nabla_x\Phi(x,y)dx\right)H'(\phi(y))\phi_1(y)dy+O(\phi_1^2)\,. \end{aligned} \tag{23}$$

Hence,

$$\frac{\partial F}{\partial\phi}=\int_{\Gamma_0}2G^T(x;\phi,g)\nabla_x\Phi(x,y)dx\delta(\phi(y)).$$

The necessary condition for ϕ to be a minimizer is

$$\begin{aligned} 0 &= \frac{\partial F}{\partial\phi}=\int_{\Gamma_0}2G(x;\phi,g)^T\nabla_x\Phi(x,y)dx\ \delta(\phi(y)), \\ 0 &= \frac{1}{|\nabla\phi|}\frac{\partial\phi}{\partial n}\quad\text{on }\partial\Omega, \end{aligned} \tag{24}$$

where we have imposed the natural boundary condition for ϕ on the boundary of Ω. If we choose $\phi_1=-\frac{\partial F}{\partial\phi}$, which is the gradient descent direction, then the functional is decreasing along the negative gradient direction. Thus we will evolve the following gradient flow to the steady state to compute the minimizer:

$$\begin{aligned} \frac{\partial\phi}{dt} &= -\frac{\partial F}{\partial\phi} \\ \frac{1}{|\nabla\phi|}\frac{\partial\phi}{\partial n} &= 0\quad\text{on }\partial\Omega, \end{aligned} \tag{25}$$

where $\phi=\phi(x,t)$ with t being the artificial evolution time. We will take $\varphi(x)=\phi(x,\infty)$ and $\partial D=\{x:\varphi(x)=0\}$.

Note, however, that the previous formulation does not incorporate the constraints that the structure now is given by $\mu=g\,d\Gamma+\chi_D$ and also that the upper surface is given explicitly by the function γ. In the level set formulation, we first convert it into an implicit representation by the following strategy. We extend the function g from the upper surface of the iceberg $\gamma(x_1,x_2)$ to Ω such that g is constant in the normal direction away from the surface $\phi^{-1}(0)$. Without causing any confusion, we will denote this extended mass function by the same notation g for the rest of the paper. Numerically, we obtain such an extension by solving

$$g_\tau+\mathrm{sgn}(\phi)\left(\frac{\nabla\phi}{|\nabla\phi|}\cdot\nabla\right)g=0\,, \tag{26}$$

where the boundary condition $g(x,\tau)$ is fixed on $\phi=0$. Since we require the solution only in a local neighborhood of the surface Γ, we do not solve this PDE until we obtain the steady state solution. In practice, we can simply solve the above hyperbolic PDE for several iterations in the τ-direction. Similar techniques have been widely used in the level set community in various applications [18, 20, 21, 22, 5].

To minimize (21), we propose the strategy of alternating minimization of the functional with respect to the level set function ϕ (corresponding to the bottom shape of the iceberg, i.e. D) and the extended mass function g. Formally we obtain

the following variation of the level set function in (21) using the property that the normal derivative of g away from the boundary of the iceberg is zero,

$$\frac{\partial F}{\partial \phi} = 2\int_{\Gamma_0} G(x;\phi,g)^T \nabla_x \Phi(x,y) dx \delta(\phi(y)) H(-y_3)$$

with G given by (22). Since the upper surface of the iceberg is given, this variation formula will be applied to ϕ for $x_3 < 0$ only.

For the alternating step to minimize the extended mass function g, we rewrite the surface integral in (13) to

$$\int_\Gamma \Phi(x,y) g(y) d\Gamma = \int_\Omega \Phi(x,y) g(y) \delta(\phi(y)) H(y_3) dy\,.$$

Now, the variation of F with respect to g in Ω is then given by

$$\frac{\partial F}{\partial g} = 2\int_{\Gamma_0} G^T(x;\phi,g) \nabla_x \Phi(x,y) dx H(y_3)\,, \tag{27}$$

and the gradient flow is given by

$$\frac{\partial g}{\partial t} = -\frac{\partial F}{\partial g}\,. \tag{28}$$

Similar to the direct approach, we also need to stabilize this gradient flow. We propose to regularize the mass function g defined on the upper surface Γ of the inclusion by adding the term $\|\nabla_\Gamma g\|^2_\Gamma$ to the functional, where the operator ∇_Γ is the surface gradient defined on Γ. The minimizer of this functional can be computed by finding the corresponding surface Laplacian, Δ_Γ, of the mass function. One possible way to compute this term numerically is to first explicitly parameterize the surface using triangulation. The gradient, or the surface Laplacian, can then be approximated using a local coordinate system at each mesh point. In this work, however, we propose an implicit approach which will naturally combine with the gradient flow in (27). The idea is based on the property that g is constant in the normal direction of the surface Γ, which implies $\Delta g|_\Gamma = \Delta_\Gamma g$ on Γ. Therefore, to regularize the gradient flow, we modify the Frechet derivative by

$$\frac{\partial F}{\partial g} = \left[\int_{\Gamma_0} G^T(x;\phi,g) \nabla_x \Phi(x,y) dx - \alpha \Delta g\right] H(y_3)\,, \tag{29}$$

for some small $\alpha > 0$. Several similar approaches have been introduced to solve various PDE's on surfaces. For example, a level set method was first introduced to solve elliptic problems on a manifold in [1]. The authors proposed a numerical projection operator to extend the diffusion operation from the interface to the whole computational space. Some other approaches can be found in [25, 2, 15, 13].

To summarize, we give the overall algorithm here.

Algorithm:

1. Initialization.
   (a) Initialize the level set function ϕ such that $\{\phi = 0\}$ matches with the given observation when $x_3 > 0$.
   (b) Initialize the mass function g for $x_3 > 0$ such that $(\mathbf{n}\cdot\nabla)g = 0$ with $\mathbf{n} = \nabla\phi/|\nabla\phi|$.
2. Compute the mismatch $G(x)$ on Γ_0.
3. Update the level set function.

(a) Compute the level set function derivative (24).
(b) Evolve the level set equation for a small time-step Δt according to (25).
(c) Reinitialize the level set function.

4. Update the mass function.
   (a) Compute the mass function derivative (29).
   (b) Update the mass function for a small time-step Δt according to (28).
   (c) Extend the function g in the normal direction of ϕ by solving (26) for several iterations in τ.
5. Iterate steps 2-4 until both ϕ and g converge.

When applying the level set method, in general it is a subtle issue how often to reinitialize the level set function during the evolution process. Here we do not intend to explore this issue; instead, we just solve the reinitialization equation for several artificial time steps.

3.3. **Fast computation of the mismatch.** In our previous work [11], we have proposed a fast algorithm of computing the mismatch term which can reduce the computational complexity from $O(N^{2n-1})$ in the full implementation to $O(N^{2n-2})$, where N is the number of grid points in each direction and n is the dimension of the computational space. For three-dimensions, the $O(N^4)$ implementation first requires a Cartesian-to-Polar map to construct an explicit representation of the target boundary using triangulation. With such explicit representation, the next step of the method computes intersections of all rays in the polar (spherical) coordinates from the measurement locations to these triangular simplexes.

In this current application, on the other hand, such strategy would not work directly. We first consider the integral in the mismatch term

$$\begin{aligned} I(x) &= \int_{\Omega_z} \nabla_x \Phi(x,y) \left[H(\phi(y)) + g(y)\delta(\phi(y))H(y_3) \right] dy \\ &= \int_{\Omega_z} \nabla_x \Phi(x,y) f(y) dy \end{aligned}$$

where $f(y) = H(\phi(y)) + g(y)\delta(\phi(y))H(y_3)$. With the level set implementation, the delta-function is approximated by a smoothed version which spreads in a small neighborhood of the zero level set of ϕ. Indeed, one might implement a sharp interface method by interpolating the function g on each triangular simplex and then summing up the corresponding contribution to the gravitation force; such an algorithm requires interpolation performed on various triangles.

In this work, we propose a new approach based on recent fast algorithms for low rank matrix approximation. Applying the trapezoidal rule to approximate the three-dimensional integral, we have

$$I(x_i) = \sum_j \nabla_x \Phi(x_i, y_j) f(y_j) \Delta x^3 \,,$$

where x_i are locations with measurements, y_j are mesh locations in the computational domain, $i = 1, \cdots, p = O(N^2)$, and $j = 1, \cdots, q = O(N^3)$. These summations can be written as matrix-vector multiplications, where all three matrices have

a similar form $\mathbf{M}^{(1)} = [M_{i,j}^{(1)}]$, $\mathbf{M}^{(2)} = [M_{i,j}^{(2)}]$ and $\mathbf{M}^{(3)} = [M_{i,j}^{(3)}]$ given by

$$M_{i,j}^{(1)} = -\frac{\Delta x^3}{4\pi} \frac{\left(x_i^{(1)} - y_j^{(1)}\right)}{\|x_i - y_j\|^3}, \; M_{i,j}^{(2)} = -\frac{\Delta x^3}{4\pi} \frac{\left(x_i^{(2)} - y_j^{(2)}\right)}{\|x_i - y_j\|^3}$$
$$\text{and} \;\; M_{i,j}^{(3)} = -\frac{\Delta x^3}{4\pi} \frac{\left(x_i^{(3)} - y_j^{(3)}\right)}{\|x_i - y_j\|^3}.$$

Direct computation of this matrix-vector multiplication requires $O(N^{2n-1}) = O(N^5)$ operations. Now, taking advantage of the fact that these matrices have simple structure, we apply the following low rank approximation using SVD. We decompose

$$\mathbf{M} = \mathbf{U}\mathbf{S}\mathbf{V}^T \approx \tilde{\mathbf{U}}\mathbf{S}^{(k)}\tilde{\mathbf{V}}^T$$

where $\mathbf{U}$ and $\mathbf{V}$ are isometric matrices of size p-by-r and q-by-r with r being the rank of the matrix $\mathbf{M}$, $\tilde{\mathbf{U}}$ and $\tilde{\mathbf{V}}$ are k-leftmost columns of $\mathbf{U}$ and $\mathbf{V}$, respectively, $\mathbf{S}$ and $\mathbf{S}^{(k)}$ are both diagonal and have the same leading k diagonal elements, where the integer k is much smaller than $\min(p, q) = O(N^2)$. Numerically, we pick $k = 4N = O(N)$ which already gives accurate solution in the current application. There are recent randomized algorithms to compute this k-rank approximation efficiently [8]. Unfortunately, since the matrix $\mathbf{M}$ is full, the computational complexity of this low rank approximation is given by $O(kpq) = O(N^{2n-1})$ which is not too appealing. However, we can treat these decompositions as a pre-processing step. We only need to compute the decomposition once and we can store in the computer memory these coefficients (there are only $O(k(p + 1 + q)) = O(N^{n+1})$ of them). With this decomposition, the integration can be approximated in $O(N^{n+1}) = O(N^4)$ operations in three dimensions.

4. Examples.

Since recovering only the density with the correct topology is more straightforward, we are not going to concentrate our effort to that aspect of the inverse problem. However, we do show an example for the level set approach on an ellipsoid; see Figure 4.2.1. In this case, the topology is correct while we can nicely recover the amount of snow on the top of the iceberg.

4.1. Direct approach.

In this example, we consider the direct approach to the inverse problem, where the bottom part of the iceberg is explicitly represented as a function of Γ'. The upper part and the lower part of the iceberg are given by the sphere of radius $R = 0.35$ centered at the origin. The exact mass function $g(x, y)$ defined on the upper surface $\gamma(x, y)$ is designed to be 0.5.

Figure 2 shows the inverted shape using our proposed direct approach. In figure 2 (a), we do not impose extra regularity on the shape and so there is a sharp edge in the solution. With extra penalty terms in the energy (18), the shape is much smoother. To better visualize the improvement, we also plot some cross-sections of the solution which are shown in figure 3. With the extra shape regularization, we are able to obtain a smoother change in the bottom shape of the iceberg.

The second part of the inverse problem is to invert the mass of a thin layer of ice on the upper iceberg. In figure 2, we color the upper surface according to the solution g. To better check the accuracy, we plot also the cross-sections of g as a function of x_1 or x_2 in figure 4. The extra penalty term in the shape regularity also slightly improves the estimate of the mass function defined on the upper surface.

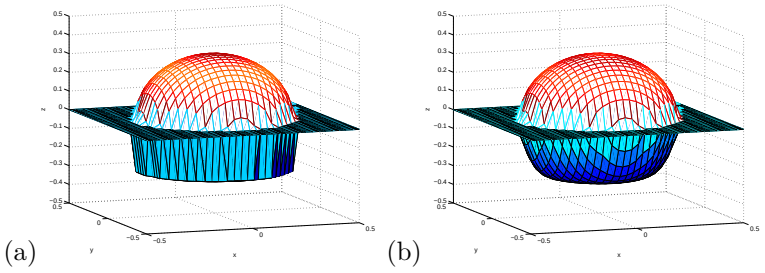

(a) (b)

FIGURE 2. (Example 4.1) Spherical iceberg with $R = 0.35$. Inverted lower surface of the iceberg computed using a mesh of 33×33 (a) without and (b) with shape regularization.

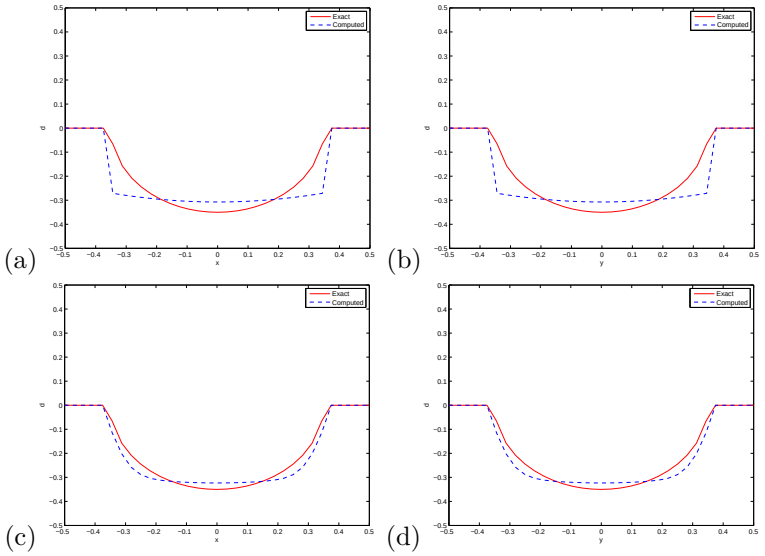

(a) (b) (c) (d)

FIGURE 3. (Example 4.1) Spherical iceberg with $R = 0.35$. Inverted lower surface of the iceberg computed using a mesh of 33×33. Without shape regularization: (a) Cross-section of the bottom iceberg along $y = 0$, i.e. $d(x, 0)$, and (b) along $x = 0$, i.e. $d(0, y)$. With shape regularization: (c) Cross-section of the bottom iceberg along $y = 0$, i.e. $d(x, 0)$, and (d) along $x = 0$, i.e. $d(0, y)$.

4.2. **Level set formulation.** Since there are limitations of the direct approach, we will concentrate on the level set formulation. One very important advantage for using the level set method is that the formulation allows topological changes in the solution. Such a variational formulation can naturally handle breaking or merging of iceberg. In this section, we will demonstrate the numerical flexibility of the proposed method in the current application.

Other than applying the low rank approximation in computing the mismatch term, to further speed up the convergence we propose also another strategy to design the initial guess for the level set iterations. We first solve the inverse problem starting from a coarse mesh using a simple initial guess. The given measurement

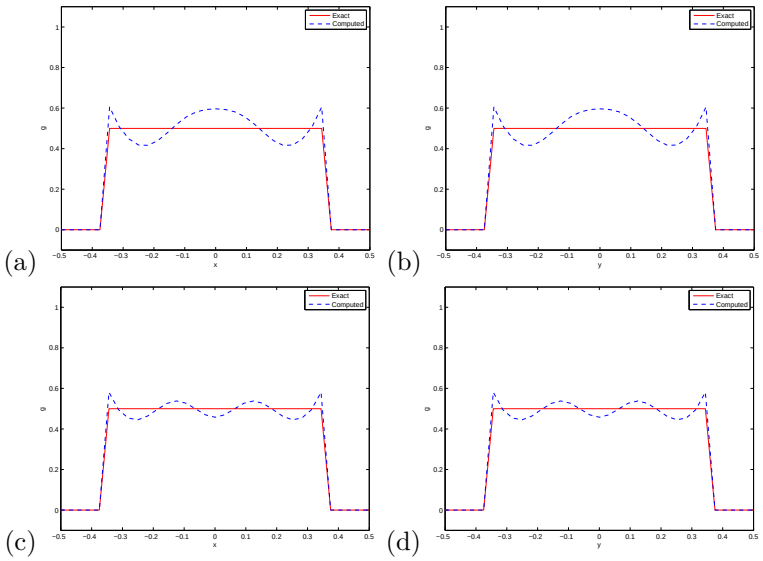

FIGURE 4. (Example 4.1) Spherical iceberg with $R = 0.35$. Mass distributed on the upper surface computed using a mesh of 33×33. Without shape regularization: (a) Cross-section of mass function on the upper iceberg along $y = 0$, i.e. $g(x, 0)$, and (b) along $x = 0$, i.e. $g(0, y)$. With shape regularization: (c) Cross-section of the mass function on the upper iceberg along $y = 0$, i.e. $g(x, 0)$, and (d) along $x = 0$, i.e. $g(0, y)$.

data are obtained by approximating the integral (19) and (20) using the trapezoidal rule on the coarse mesh *without* applying the low rank approximation. Although the initial conditions might be very different from the exact solution, the computation is very fast and we can afford to take many iterations. Once we have obtained the numerical solution, we interpolate the level set function on a finer mesh and use it as the initial condition for computing a higher resolution solution.

In the following examples, we assume two separated sets of measurements. The first set of data are given on the sky level $x_3 = 0.35$ at all mesh locations in the computational domain $\{(x_1, x_2) \in [-0.5, 0.5]^2\}$. Therefore, there are only 33^2 measurement locations on a 33^3 mesh. The second case is that measurement data are given on both the sky level $x_3 = 0.35$ and also the ground/water surface level outside the iceberg(s). Although the number of measurements is less than double of the previous set, these extra measurements are shown to be providing important information for the reconstruction.

4.2.1. *Ellipsoidal iceberg.* The first example is a small variation of the previous example where we now replace the sphere by an ellipsoid and the constant mass distribution by a slightly more realistic mass function where it is close to zero on the edge of the iceberg and is more concentrated at the center of the upper surface. Mathematically, the exact ellipsoidal surface is given by

$$\left(\frac{x_1}{0.35}\right)^2 + \left(\frac{x_2}{0.35}\right)^2 + \left(\frac{x_3}{0.2}\right)^2 = 1\,,$$

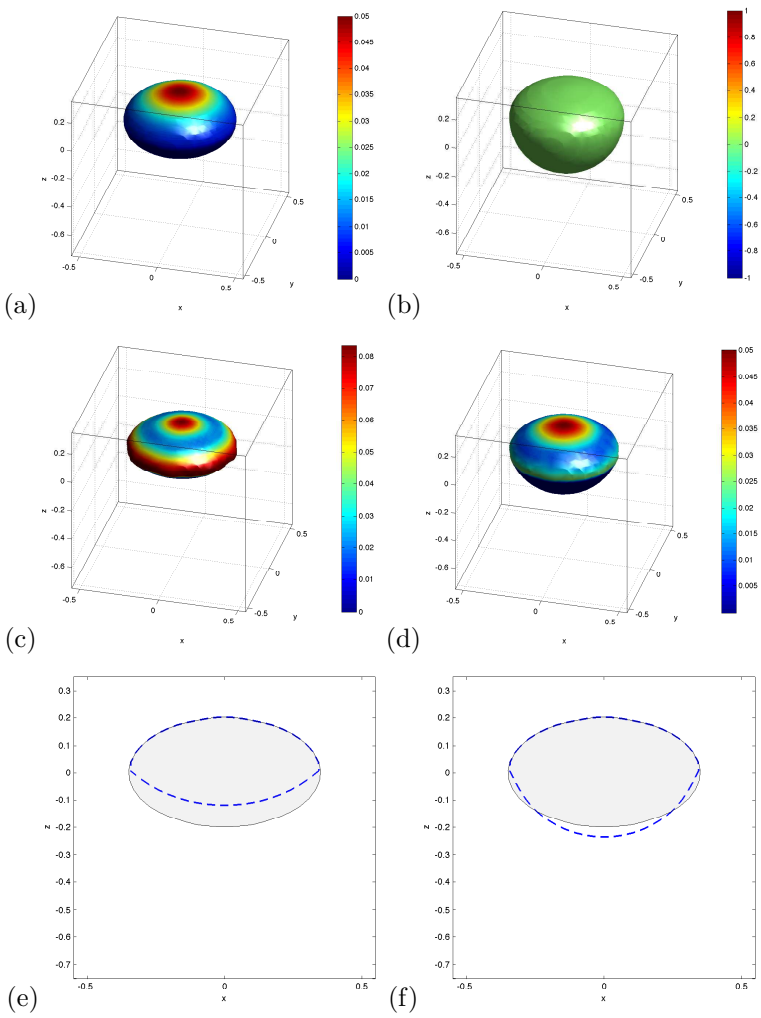

Figure 5. (Example 4.2.1) The inverted solution using 33^3 mesh *without* the low rank approximation in computing the mismatch integral. (a) The exact solution. (b) The initial guess. Solutions with measurements on (c) the sky level ($x_3 = 0.35$) and (d) both the sky level and the ground level ($x_3 = 0$). Cross-sections along $y = 0$ with measurements given on (e) the sky level ($x_3 = 0.35$)and (f) both the sky level and the ground level ($x_3 = 0$).

and the mass distributed on the upper surface is

$$g(x_1, x_2) = 0.05 \exp\left(-\frac{x_1^2 + x_2^2}{2\sigma^2}\right),$$

where $\sigma = 0.1$. This exact solution is plotted in figure 5 (a).

In this example, we fix the number of mesh points in each dimension to be 33 and we do not apply multiple sets of meshes to speed up the computation. The initial guess below the water surface is a lower-half sphere of radius 0.35, figure 5 (b). In

figure 5(c), we show the solution obtained using measurements imposed only on the sky level $x_3 = 0.35$. Together with measurements on the ground level $x_3 = 0$ outside the iceberg, the mass distribution on the upper iceberg is much improved, figure 5 (d). The shape of the under-water surface is also improved. We plot the cross sections of these solutions along the line $y = 0$ in figure 5 (e-f). The exact shapes are plotted in shaded colors in these figures while the computed solutions are plotted in dashed lines. With only measurements on the sky level, the enclosed volume in the inverted solution is under-estimated; to better match with the measurements, the mass distribution is slightly over-estimated; see figure 5 (c).

4.2.2. *Two ellipsoidal icebergs.* This example is to demonstrate that the level set formulation can naturally split a big iceberg into several smaller ones to better match with the measurements. The exact solution consists of two disconnected icebergs where each of them has a spherical upper surface of radius $r = 0.2$ centered at $(0.175, 0.175)$ and $(-0.175, -0.175)$, and an ellipsoidal lower surface of the longer semiaxis with length given by 0.4, figure 6 (a). The initial condition is a connected torus-shaped surface with the mass function being zero everywhere; see figure 6 (b).

Figure 6 (c) shows the solution with measurements given only on the sky level $x_3 = 0.35$. Similar to the previous example, the algorithm under-estimates the volume enclosed but over-estimates the mass distribution on the upper surface of the iceberg. With extra measurements given on the ground level outside the iceberg, the solution (both the lower shape and also the mass distribution on the upper surface) is much improved, as shown in figure 6 (d).

To further speed up the computations, we apply the low rank approximation to the mismatch integral and also use the iterative procedure by using the solution from a coarser mesh as an initial condition for the finer mesh computation. Figure 6 (e) shows the solutions for 65^3 meshes with given measurements only on the sky level $x_3 = 0.35$. Figure 6 (f) shows the corresponding solution with extra measurements given on the ground level outside the iceberg surface. Even though this solution is less accurate than the full implementation as in (d), these solutions are qualitatively similar to what we obtained before.

4.2.3. *Discovering connectivity.* Opposite to the previous example, this case is to show that the level set formulation could discover hidden connectivity under the sea surface. In practice, one can observe those surfaces only if they are above the sea surface. In this example, we assume that the given surfaces are upper half-spheres centered at $(0.175, 0.175)$ and $(-0.175, -0.175)$ with radius 0.2, figure 7 (a). To test the capability of the level set method for recovering the correct topology in the solution, we take an initial condition which has a different topology from the exact solution and is shown in Figure 7 (b). And we would like to test if our proposed method could automatically merge these surfaces and give a topologically correct solution. Since the connected region is completely immersed under the sea surface, the direct approach proposed in Section 3.1 is not able to determine such a solution.

Figure 7 (c) shows the inverted solution using only measurements given on the sky level $x_3 = 0.35$, where the mismatch integral is computed without applying the low rank approximation. With very little information given, the iceberg does not merge but the algorithm puts more mass on the upper surface of the iceberg to compensate for the missing underwater mass connecting these two objects. With extra information provided on the ground level, the algorithm is able to connect these two objects and give a topologically correct solution.

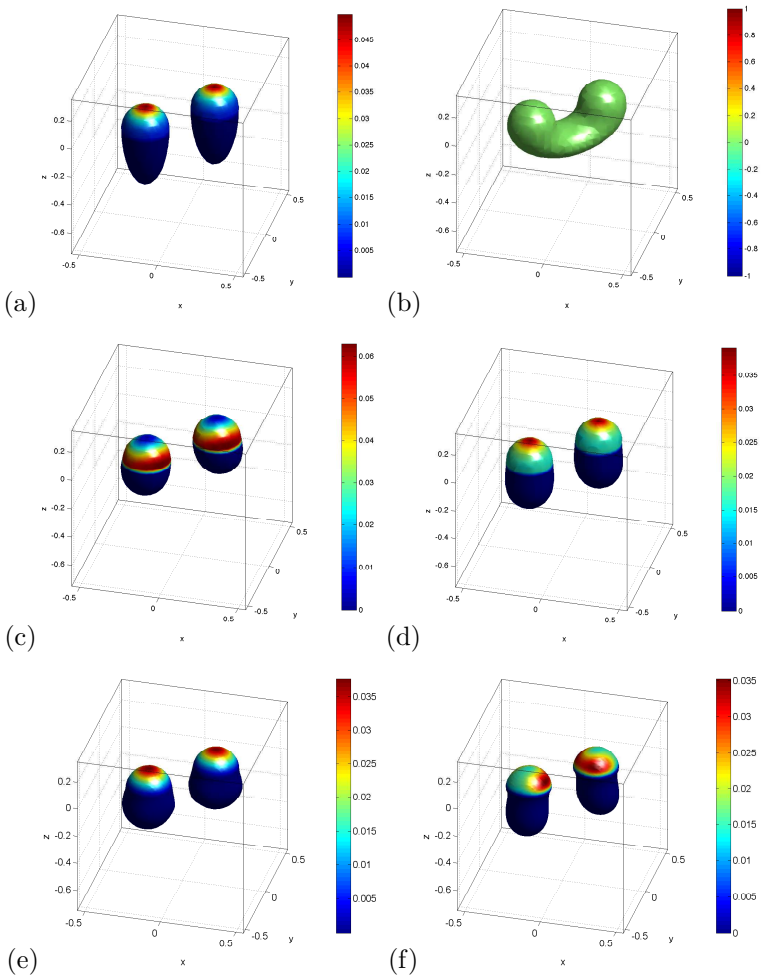

Figure 6. (Example 4.2.2) (a) The exact solution in 33^3 mesh. (b) The initial guess. The inverted solution *without* the low rank approximation in computing the mismatch integral: Measurements given on the sky level ($x_3 = 0.35$) and (d) both the sky level and the ground level ($x_3 = 0$). The inverted solutions on the 65^3 mesh *with* the low rank approximation in computing the mismatch integral: Measurements given on (e) the sky level ($x_3 = 0.35$) and (f) both the sky level and the ground level ($x_3 = 0$).

We follow a similar procedure as in the previous case to speed up the fine mesh computations. Figures 7 (e-f) show the solutions on a 65^3 mesh using the low rank approximation in the mismatch functional with measurements only on the sky level (figure 7 (e)) and on both the sky level and the ground level (figure 7 (f)). As in the previous example, we are able to efficiently obtain the inverted solution using a fine mesh by applying the low rank approximation to the mismatch integral and

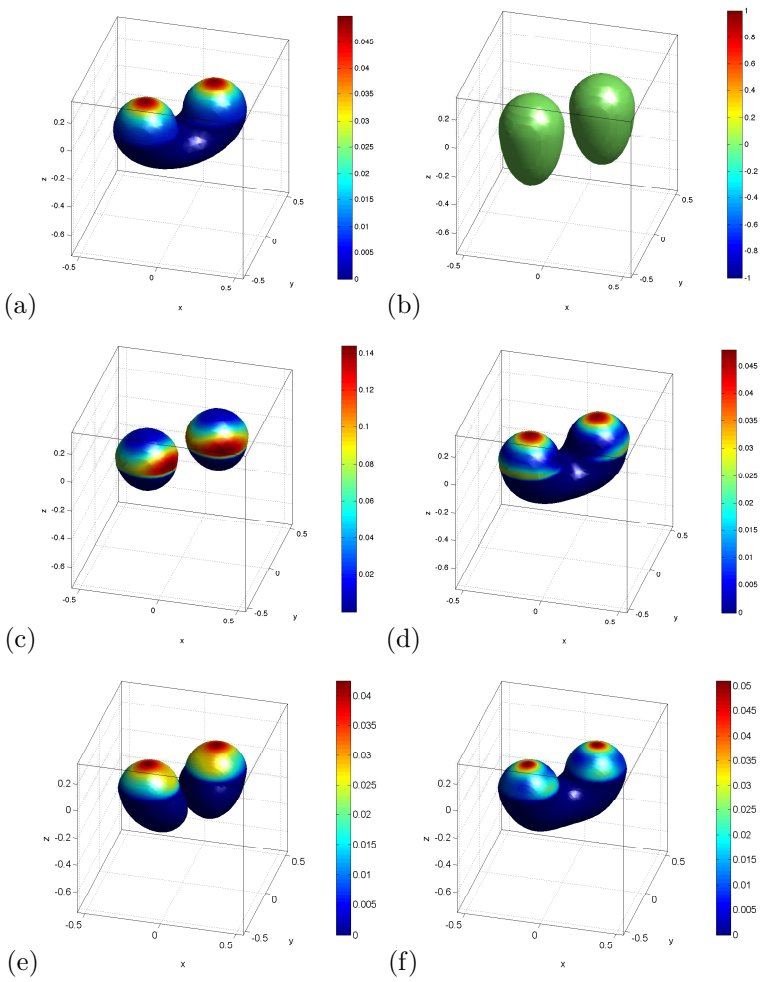

FIGURE 7. (Example 4.2.3) (a) The exact solution in 33^3 mesh. (b) The initial guess. The inverted solution *without* the low rank approximation in computing the mismatch integral: Measurements given on (c) the sky level ($x_3 = 0.35$) and (d) both the sky level and the ground level ($x_3 = 0$). The inverted solutions on the 65^3 mesh *with* the low rank approximation in computing the mismatch integral: Measurements given on (e) the sky level ($x_3 = 0.35$) and (f) both the sky level and the ground level ($x_3 = 0$).

picking a better initial guess for the iterations. The solutions are qualitatively the same as those by the full implementation.

We remark that although the geometry is rather simple in all these examples, it is sufficient to demonstrate the capability of the proposed method to recover the quantity of snow and the topology of the iceberg, which is the most important in practice.

5. **Conclusion.** We introduced a model of floating ice D with snow cap. We demonstrated uniqueness of recovering D and snow thickness from the remote measurements of their gravitational potential under mild and seemingly minimal assumptions on D. We designed and tested two different numerical algorithms for finding D and snow thickness. Due to the analysis of the stability of the harmonic continuation in [7] it is realistic to find in a stable way at most 10-15 parameters describing D and g. So we expect to recover D slightly more general than ellipsoids.

Goals for the near future are to understand resolution limits of our numerical methods in terms of dependence on data errors, the collection set $\mathcal{A}$ of measurements, sizes of measurement site Γ_0 and sizes of domain D, and on the distance from Γ_0 to D. Then one of the main challenges is to apply our methods to realistic data and compare recovered D with (geo) physical reality. Since the density of the sea water is nearly constant, we have a fortunate situation of a known background.

Another challenge is to develop a suitable model for floating ice touching the sea bottom, where ice can be identified from exterior gravity data, and to design appropriate numerical methods for the related inverse problem.

Acknowledgments. Isakov's research was in part supported by NGA, NSF, and by Emylou Keith and Betty Dutcher Distinguished Professorship at WSU. Leung was supported in part by Hong Kong RGC under Grant GRF603011 and and HKUST RPC under Grant RPC11SC06. Qian's research is partially supported by NGA and NSF.

REFERENCES

[1] M. Bertalmio, L.-T. Cheng, S. Osher and G. Sapiro, *Variational problems and partial differential equations on implicit surfaces*, J. Comput. Phys., **174** (2001), 759–780.
[2] J. Brandman, *A level-set method for computing the eigenvalues of elliptic operators defined on compact hypersurfaces*, J. Sci. Comput., **37** (2008), 282–315.
[3] M. Burger, *A level set method for inverse problems*, Inverse Problems, **17** (2001), 1327–1356.
[4] M. Burger and S. Osher, *A survey on level set methods for inverse problems and optimal design*, European J. Appl. Math., **16** (2005), 263–301.
[5] T. Cecil, S. J. Osher and J. Qian, *Simplex free adaptive tree fast sweeping and evolution methods for solving level set equations in arbitrary dimension*, J. Comput. Phys., **213** (2006), 458–473.
[6] O. Dorn and D. Lesselier, *Level set methods for inverse scattering*, Inverse Problems, **22** (2006), R67–R131.
[7] A. Elcrat, V. Isakov, E. Kropf and D. Stewart, *A stability analysis of the harmonic continuation*, Inverse Problems, **28** (2012), 075016.
[8] N. Halko, P. G. Martinsson, Y. Shkolnisky and M Tygert, *An algorithm for the principal component analysis of large data sets*, SIAM J. Sci. Comput., **33** (2010), 2580–2594.
[9] S. Hou, K. Solna and H.-K. Zhao, *Imaging of location and geometry for extended targets using the response matrix*, J. Comput. Phys., **199** (2004), 317–388.
[10] V. Isakov, "Inverse Source Problems," AMS, Providence, 1990.
[11] V. Isakov, S. Leung and J. Qian, *A fast local level set method for inverse gravimetry*, Commun. Comput. Phys., **10** (2011), 1044–1070.
[12] M. Keldysh, *On the solubility and stability of the Dirichlet's problem*, Uspekhi Matem. Nauk., **8** (1940), 171–231.
[13] S. Leung, *Eulerian approach for computing the finite time Lyapunov exponent*, J. Comput. Phys., **230** (2011), 3500–3524.
[14] A. Litman, D. Lesselier and F. Santosa, *Reconstruction of a 2-D binary obstacle by controlled evolution of a level-set*, Inverse Problems, **14** (1998), 685–706.
[15] C. B. Macdonald and S. J. Ruuth, *The implicit closest point method for the numerical solution of partial differential equations on surfaces*, SIAM J. Sci. Comput., **31** (2009), 4330–4350.

[16] C. Miranda, "Partial Differential Equations of Elliptic Type," Springer-Verlag, New York-Berlin, 1970.
[17] P. Novikov, *Sur le probleme inverse du potential*, Dokl. Akad. Nauk SSSR, **18** (1938), 165–168.
[18] S. J. Osher and J. A. Sethian, *Fronts propagating with curvature dependent speed: algorithms based on Hamilton-Jacobi formulations*, J. Comput. Phys., **79** (1988), 12–49.
[19] A. I. Prilepko, D. G. Orlovskii and I. A. Vasin, "Methods for Solving Inverse Problems in Mathematical Physics," Marcel Dekker, New York, 2000.
[20] J. Qian, L.-T. Cheng and S. J. Osher, *A level set based Eulerian approach for anisotropic wave propagations*, Wave Motion, **37** (2003), 365–379.
[21] J. Qian and S. Leung, *A level set method for paraxial multivalued traveltimes*, J. Comput. Phys., **197** (2004), 711–736.
[22] J. Qian and S. Leung, *A local level set method for paraxial multivalued geometric optics*, SIAM J. Sci. Comp., **28** (2006), 206–223.
[23] F. Santosa, *A level-set approach for inverse problems involving obstacles*, Control, Optimizat. Calculus Variat., **1** (1996), 17–33.
[24] K. van den Doel, U. Ascher and A. Leitao, *Multiple level sets for piecewise constant surface reconstruction in highly ill-posed problems*, J. Sci. Comput., **43** (2010), 44–66.
[25] J. Xu and H. K. Zhao, *An Eulerian formulation for solving partial differential equations along a moving interface*, J. Sci. Comput., **19** (2003), 573–594.
[26] H.-K. Zhao, T. Chan, B. Merriman and S. J. Osher, *A variational level set approach for multiphase motion*, J. Comput. Phys., **127** (1996), 179–195.

Received September 2012; revised February 2013.

E-mail address: victor.isakov@wichita.edu
E-mail address: masyleung@ust.hk
E-mail address: qian@math.msu.edu